Published in final edited form as:
J Am Chem Soc. 2013 June 12; 135(23): . doi:10.1021/ja3104632.

In-situ X-Ray Absorption Spectroscopy (XAS) Investigation of a Bifunctional Manganese Oxide Catalyst with High Activity for Electrochemical Water Oxidation and Oxygen Reduction

Yelena Gorlin[#a], **Benedikt Lassalle-Kaiser**[#b,†], **Jesse D. Benck**[a], **Sheraz Gul**[b], **Samuel M. Webb**[c], **Vittal K. Yachandra**[b], **Junko Yano**[b,*], and **Thomas F. Jaramillo**[a,*]

[a]Department of Chemical Engineering, Stanford University, Stanford, CA 94305

[b]Physical Biosciences Division, Lawrence Berkeley National Laboratory Berkeley, CA 94720

[c]Stanford Synchrotron Radiation Lightsource, SLAC National Accelerator Laboratory, Menlo Park, CA, 94025

[#] These authors contributed equally to this work.

Abstract

In-situ x-ray absorption spectroscopy (XAS) is a powerful technique that can be applied to electrochemical systems, with the ability to elucidate the chemical nature of electrocatalysts under reaction conditions. In this study, we perform *in-situ* XAS measurements on a bifunctional manganese oxide (MnO_x) catalyst with high electrochemical activity for the oxygen reduction reaction (ORR) and the oxygen evolution reaction (OER). Using x-ray absorption near edge structure (XANES) and extended x-ray absorption fine structure (EXAFS), we find that exposure to an ORR-relevant potential of 0.7 V vs. RHE produces a disordered $Mn_3^{II,III,III}O_4$ phase with negligible contributions from other phases. After the potential is increased to a highly anodic value of 1.8 V vs. RHE, relevant to the OER, we observe an oxidation of approximately 80% of the catalytic thin film to form a mixed $Mn^{III,IV}$ oxide, while the remaining 20% of the film consists of a less oxidized phase, likely corresponding to unchanged $Mn_3^{II,III,III}O_4$. XAS and electrochemical characterization of two thin film catalysts with different MnO_x thicknesses reveals no significant influence of thickness on the measured oxidation states, at either ORR or OER potentials, but demonstrates that the OER activity scales with film thickness. This result suggests that the films have porous structure, which does not restrict electrocatalysis to the top geometric layer of the film. As the portion of the catalyst film that is most likely to be oxidized at the high potentials necessary for the OER is that which is closest to the electrolyte interface, we hypothesize that the $Mn^{III,IV}$ oxide, rather than $Mn_3^{II,III,III}O_4$, is the phase pertinent to the observed OER activity.

INTRODUCTION

The development of catalytic materials for the oxygen reduction reaction (ORR) and the oxygen evolution reaction (OER) is one of the major challenges in electrochemical energy conversion and storage technologies such as fuel cells, metal-air batteries, electrolysis cells, and solar fuel synthesis reactors. To implement strategies for the rational design of catalysts for the ORR and the OER, it is important to improve understanding of the chemical state and

[*]Corresponding authors, jyano@lbl.gov, jaramillo@stanford.edu.
[†]**Present Address** Synchrotron SOLEIL, L'Orme des Merisiers, BP 42 Saint-Aubin *91192, Gif-sur-Yvette, France.*

Supporting Information. X-ray photoelectron spectroscopy analysis, x-ray absorption spectroscopy fitting details, Figures S1-S8. This material is available free of charge via the Internet at http://pubs.acs.org.

structure of active surfaces under reaction conditions. X-ray absorption spectroscopy (XAS) can be combined with electrochemistry to elucidate the properties of catalytic materials *in-situ*. X-ray absorption near edge structure (XANES) probes the electronic structure of the catalyst, while the extended x-ray absorption fine structure (EXAFS) probes the bond geometry and coordination of the catalysts. In the past, *in-situ* XAS measurements have been applied to a variety of ORR and OER catalyst systems. For example, *in-situ* XAS measurements have been used to track the oxidation state of platinum as a function of potential in the ORR region,[1] correlate d-band vacancies on platinum alloy catalysts to oxygen reduction activity,[2] and link higher $Mn^{IV}O_2$ content to better ORR performance in MnO_x catalysts.[3,4] The method has also been used to understand the valency and structure of cobalt phosphate and nickel borate OER catalysts[5,6] and investigate photochemical oxygen evolution on a tetranuclear manganese cluster.[7]

Only a few *in-situ* XAS studies, however, have described changes in the active catalyst phase between the ORR and OER regimes using the same material.[8] The significant overpotentials associated with these two reactions make it unlikely that the same surface phase will form under both reductive and oxidative potentials.[9] Because of the large number of MnO_x phases that may be associated with high ORR[4,10-13] and OER activities,[14-16] it could be possible for MnO_x-based catalysts to change surface structure as a function of potential and still exhibit high activity for both reactions. In our work, we performed *in-situ* XAS measurements on a bifunctional manganese oxide (MnO_x) catalyst with high electrochemical activity for both the ORR and the OER. To prepare a bifunctional MnO_x catalyst, we adopted a synthesis procedure previously developed for the deposition of MnO_x on glassy carbon (GC)[13] to deposition on a gold-coated silicon nitride (Au-Si_3N_4) window. Using information from *in situ* XANES and EXAFS we found that the switch from ORR to OER potentials results in a structural change in the MnO_x/Au-Si_3N_4 catalyst and characterized the MnO_x phases present under each set of conditions. We also studied samples with two different thicknesses of the catalytic layer to investigate the porosity and electrochemical accessibility of the MnO_x films. Our results link specific Mn oxide phases to ORR and OER conditions, thus increasing understanding of oxygen electrocatalysis on MnO_x electrodes.

EXPERIMENTAL SECTION

Electrodeposition of Manganese Oxide Catalyst

Prior to manganese oxide (MnO_x) electrodeposition, silicon nitride membrane (Si_3N_4) windows (1000 nm membrane, Silson Ltd.) were sputter coated with a 10 nm binding layer of titanium and a 100 nm layer of gold to produce a suitable electrode substrate (Au Si_3N_4). The catalyst was synthesized via a previously reported procedure.[13,17] The electrolyte used for deposition was prepared by dissolving 0.71 g of sodium sulfate (Sigma-Aldrich, >99.0%) and 1.23 g of manganous acetate (Aldrich, 99.99%) in 50 mL of Millipore water at room temperature, yielding a solution with pH of 7.4. The solution was then aged for 6 days, until the pH dropped to approximately 7. Manganese oxide was electrodeposited in a three electrode electrochemical cell using the Au-Si_3N_4 substrate contacted by copper tape as the working electrode, a Ag|AgCl reference electrode, and a graphite foil counter electrode. Before performing electrodeposition, the resistance between the working and reference electrodes was measured to ensure proper electrical contact between copper tape and the gold layer of Au-Si_3N_4. After establishing a proper contact and achieving a resistance of 30-60 Ω, the potential was iR compensated to 85% and cycled nine times between 0.0 and 0.6 V vs Ag|AgCl at a sweep rate of 20 $mV \cdot s^{-1}$. The Au-Si_3N_4 membrane coated with the resulting thin film was placed in a ceramic boat (Fisher Scientific) and heat treated in air at 480°C for 10 hours in a tube furnace (Mellen Company SC13).

Electrochemical Characterization

The electrochemical activity of the electrodeposited MnO_x thin film was first evaluated using cyclic voltammetry in a three-electrode electrochemical cell. All cyclic voltammograms (CVs) were iR-compensated to 85% and measured in 0.1 M KOH electrolyte at 23°C with a sweep rate of 20 $mV \cdot s^{-1}$, using a carbon rod counter electrode and a Ag|AgCl reference electrode. The electrolyte (0.1 M KOH) was prepared from high purity KOH pellets (Sigma-Aldrich, 99.99%) by adding 5.60 g of pellets to 1 L of Millipore water. The potential scale was calibrated to a reversible hydrogen electrode (RHE) at the end of the catalyst characterization in a hydrogen saturated electrolyte with platinum nanoparticles as the working electrode (20-wt.% Pt on Vulcan XC-72, Etek). The potential of 0.960 V at which the current crossed zero was taken to be the thermodynamic potential for the hydrogen electrode reactions. All potentials during electrochemical characterization are reported vs. RHE. To characterize the activity of the catalyst for the oxygen evolution reaction (OER) and the oxygen reduction reaction (ORR), CVs were performed over a potential range of 0.05 V to 1.8 V in an oxygen saturated environment. Additional CVs were performed from 0.05 to 1.1 V in oxygen and nitrogen saturated environments to confirm the electro-catalytic activity of the catalyst for the ORR.

Physical Characterization

The morphology of the MnO_x catalyst was studied using scanning electron microscopy (SEM, FEI Magellan 400 XHR). A 25 pA beam current of 5 kV and a secondary electron detector were used. The crystal structure of MnO_x catalyst was investigated using x-ray diffraction with Cu Kα1 radiation and λ=1.54 Å, operated at 45 kV and 40 mA (XRD, Phillips X'Pert 2). 2θ scans from 10° to 90° were performed on the catalyst and the bare Au-Si_3N_4 substrate, at a scan speed of 0.02°·s^{-1}.

Ex-situ XPS Characterization

The manganese oxidation state and potassium intercalation were studied by x-ray photoelectron spectroscopy using monochromated Al Kα 1486.6 eV x-rays (XPS, PHI 5000 VersaProbe). Three samples were investigated: an as-prepared sample, an ORR relevant sample, and an OER relevant sample. To prepare the ORR and OER relevant samples, MnO_x on Au-Si_3N_4 was cycled from 0.05 V vs. RHE to a vertex potential of either 0.70 or 1.8 V vs. RHE, held at the vertex potential for 10 minutes, extracted from the electrochemical cell under potential control, and characterized using XPS. During the *ex-situ* XPS characterization, the high resolution spectra in Mn 2p, Mn 3s, and C 1s/K 2p regions were obtained on the MnO_x catalysts, and four powder standards: $Mn^{II}O$, $Mn_3{}^{II,III,III}$, $Mn_2{}^{III}O_3$, and $Mn^{IV}O_2$ (Sigma-Aldrich). $Mn_3{}^{II,III,III}{}^{III}O_4$, $Mn_2{}^{III}O_3$, and $Mn^{IV}O_2$ powders were used as received, while $Mn^{II}O$ powder was sputtered prior to collecting XPS spectra to remove the oxidized surface known to form on $Mn^{II}O$ in air.[18] All spectra were collected using a pass energy of 23.5 eV, an energy step of 0.1 eV, and a time of 20 ms per step and were calibrated to the position of adventitious carbon at 285.0 eV.[19] The specific energy windows and the number of scans used to acquire each high resolution spectrum are provided in Table S1. Details describing XPS data analysis are provided in Supporting Information (SI). To monitor changes in the Mn oxidation state of MnO_x catalyst, we looked at the distance between Mn $2p_{1/2}$ peak and its satellite ($\Delta 2p_{1/2}$) and the magnitude of the Mn 3s multiplet splitting (ΔE3s), which have been previously shown to either increase ($\Delta 2p_{1/2}$) or decrease (ΔE3s) with increasing Mn oxidation state in powder standards.[20,21] This trend is especially clear when using $Mn^{II}O$, $Mn_2{}^{III}O_3$, and $Mn^{IV}O_2$ powders, representing Mn^{II}, Mn^{III}, and Mn^{IV} oxidation states, while inclusion of additional phases, such as $Mn_3{}^{II,III,III}O_4$, does not offer a greater ability to discriminate between the oxidation states.[21,22] The Mn 2p and the Mn 3s spectra of $Mn_3{}^{II,III,III}O_4$ are characterized by broader

peaks and its $2p_{1/2}$ satellite position falls between $Mn_2^{III}O_3$ and $Mn^{IV}O_2$, despite its lower oxidation state than that of either $Mn_2^{III}O_3$ or $Mn^{IV}O_2$.[20,21] For comparison we collected the spectra of $Mn_3^{II,III,III}O_4$ powder and present it alongside the other standards. In agreement with previous reports, we find that for our catalyst samples, XPS alone is not sufficient to distinguish between the $Mn_2^{III}O_3$ and $Mn_3^{II,III,III}O_4$ phases.

In-situ Mn K-edge XAS

X-ray absorption spectra (XAS) were collected at the Advanced Light Source (ALS) on beamline 10.3.2[23] with an electron energy of 1.9 GeV and an average current of 500 mA. The radiation was monochromatized by a Si (111) double-crystal monochromator. The intensity of the incident X-ray was monitored by an N_2-filled ion chamber (I_0) in front of the sample. Fluorescence spectra were recorded using a seven-element Ge solid-state detector. For electrochemical experiments, no transmission data could be collected. The energy was therefore calibrated using a glitch in the I_0 relative to the absorption edge of Mn foil, as is commonly employed in XAS experiments. All data were collected at room temperature. Data reduction of the XAS spectra was performed using custom-made software. Pre-edge and post-edge contributions were subtracted from the XAS spectra, and the results were normalized with respect to the edge jump. Background removal in *k*-space was achieved through a five-domain cubic spline. Curve fitting was performed with Artemis and IFEFFIT software using ab initio-calculated phases and amplitudes from the program FEFF 8.2.[24,25] The details of curve fitting are discussed in SI. A schematic of the *in-situ* setup is shown in Figure 1. In this setup, the back side of the Si_3N_4 window was exposed to x-rays, while the front side of the Si_3N_4 window with electrodeposited MnO_x on Au/Ti layer faced into the interior of the electrochemical cell. Electrochemistry was performed using a Ag|AgCl reference electrode, a platinum wire counter electrode, and 0.1 M KOH electrolyte exposed to ambient air. Although RHE calibration was not performed during *in-situ* XAS characterization, we assumed the same shift of 0.960 V for the Ag|AgCl reference electrode and report all potentials vs. RHE. After preparing the electrochemical cell for *in-situ* XAS measurements, the resistance between the working and reference electrodes was measured to ensure proper electrical contact between the potentiostat and MnO_x on Au-Si_3N_4. After achieving a resistance of 150 Ω, a CV was performed from 0.05 to 1.1 V to record the electrochemical features of the working electrode. During *in-situ* XAS at ORR relevant conditions, the potential was held at 0.7 V for 3.4 hours. After the completion of the measurement, the resistance between the working and reference electrodes was measured to be 73 Ω and iR-compensated cyclic voltammetry was performed from 0.05 V to 1.8 V to record bi-functional OER/ORR activity of the working electrode. During *in-situ* XAS at OER relevant conditions, the iR-compensated potential was held at 1.8 V for 5 hours. The solutions were not stirred during the measurements. After each potential change, the system was allowed to equilibrate for 5 min. Spectra were acquired in Quick-EXAFS (QXAS) mode. For the thick (9 cycles) samples, 4 sets of 20 spectra each lasting 3 minutes were recorded. For the thin samples (1 cycle), 20 sets of 20 spectra that lasted 3 minutes each were recorded. No spectral changes were observed between the first and last spectrum of a series of 20 scans or between the first and last sets of spectra, as shown in Figures S1 and S2. Typical EXAFS spectra demonstrating the signal to noise for each electrochemical condition are provided in Figure S3.

The collected XAS spectra of MnO_x on Au-Si_3N_4 were compared to *ex-situ* XAS spectra of model MnO_x compounds, including $Mn^{II}O$, $Mn_3^{II,III,III}O_4$, alpha-$Mn_2^{III}O_3$, gamma-$Mn^{III}OOH$, beta-$Mn^{IV}O_2$, and Mg^{2+} birnessite. $Mn^{II}O$ and $Mn_3^{II,III,III}O_4$ powders were obtained from Sigma-Aldrich and used as purchased. Beta-$Mn^{IV}O_2$ and alpha-$Mn_2^{III}O_3$ phases were prepared by dissolving $Mn(NO_3)_2{\cdot}H_2O$ in water, drying the solution at 60 °C for 24 hours, and calcining the powder for 3 hours at 200 °C or 500 °C, respectively.

Gamma-$Mn^{III}OOH$ powder was synthesized by preparing a solution consisting of 8 mM $MnSO_4$ and 8 mM $NH_4S_2O_8$, adjusting it to pH10 using 1 M NaOH, and heating it in a sealed autoclave at 120°C for 10 hours; the resulting powder was then washed and dried under vacuum. Powder XRD was used to confirm the phase of each synthesized compound (Figure S4). The details of Mg^{2+} birnessite syn- for deposition of MnOx catalyst onto a glassy carbon (GC) support.13 The resulting electrode, MnOx/Au-Si3N4, exhibited the expected bifunctional activity for both oxygen evolution reaction (OER) and oxygen reduction reaction (ORR) in alkaline electrolyte. The OER activity was confirmed by the formation of visible oxygen bubbles on the electrode surface at high oxidizing potentials, while the ORR activity was confirmed by performing additional characterization in both nitrogen and oxygen thesis and powder XRD characterization are described in a previously published study by Webb and co-workers.[26] Table S2 in the SI provides a summary of all the standards used in this work as well as other MnO_x phases mentioned in the text.

RESULTS AND DISCUSSION

MnO_x/Au-Si_3N_4 Catalyst

To investigate the material properties of an active manganese oxide (MnO_x) catalyst under reaction conditions, we prepared MnO_x on a gold-coated silicon nitride membrane (Au-Si_3N_4) following a previously developed procedure saturated electrolytes, which showed a significant increase in the reductive current in the presence of oxygen (Figure S5). To verify that MnO_x is the active species responsible for the OER and the ORR, we compared the catalytic activity of MnO_x/Au-Si_3N_4 to that of the bare support, Au-Si_3N_4 (Figure 2A). The catalyst clearly out-performs the bare gold support for the OER, but demonstrates similar ORR activity to Au-Si_3N_4. To deconvolute the contributions from MnO_x and Au in the observed ORR activity of the MnO_x/Au-Si_3N_4 catalyst, we examined the cyclic voltammograms of MnO_x/Au-Si_3N_4 and bare Au-Si_3N_4 in the potential region from 1.0 V to 1.4 V, where gold oxidation and reduction features are prominent.[27] The electrochemical behavior of the electrodes, plotted in the inset of Figure 2A, demonstrates that the surface in MnO_x/Au-Si_3N_4 catalyst does not display significant redox features characteristic to gold, indicating that the Au is electrochemically inaccessible. This finding links the observed ORR activity of MnO_x/Au-Si_3N_4 to the MnO_x surface. Comparison of the bifunctional oxygen electrode activity of MnO_x/Au-Si_3N_4 to the previously reported activity of MnO_x/GC (Figure S6) demonstrates that the two catalysts have similar catalytic activity when normalized to the geometric surface area.

ex-situ XPS characterization of MnO_x/GC determined that the catalyst deposits as Mn(III) oxide13 and that the possible changes to the surface oxidation state after an application of the ORR or the OER relevant potentials are too small to be detected by ex-situ XPS.[28] Similar *ex-situ* XPS characterization of MnO_x/Au-Si_3N_4 surface shown in Figure 3 reveals important differences between MnO_x deposited Au-Si_3N_4 and GC. In Figure 3A, we compare the Mn 2p spectra of MnO_x/Au-Si_3N_4 and MnO_x/GC to the spectra of powder controls. Unlike the spectrum of MnO_x/GC, which has similarities to the spectrum of $Mn_2^{III}O_3$, the spectrum of MnO_x/Au-Si_3N_4 has characteristics of two different spectra corresponding to $Mn^{II}O$ and $Mn^{IV}O_2$. The $Mn^{II}O$ characteristics are established by the peak at 640 eV, a corresponding shoulder at 651 eV, and small satellite features illustrated more clearly in Figure S8, while the $Mn^{IV}O_2$ characteristics are demonstrated by the peak at 658 eV and the satellite feature approximately 12.0 eV on the high binding energy side of the $2p_{1/2}$ peak. To confirm that as-prepared MnO_x/Au-Si_3N_4 consists of two different phases, we also compare the Mn 3s spectrum of MnO_x/Au-Si_3N_4 to the spectra of MnO_x/GC and four powder controls in Figure 3B. We find that in addition to gold 4f peaks, which overlap with Mn 3s features, the Mn 3s spectrum contains two separate multiplets with Δ3s values

similar to those of $Mn^{II}O$ and $Mn^{IV}O_2$, providing strong evidence that the catalyst deposits as a mixture of two phases.

Analysis of the effect of applied potential on the surface oxidation properties of MnO_x/Au-Si_3N_4 shown in Figures Although the MnO_x/Au-Si_3N_4 exhibits similar activity to the MnO_x/GC studied previously, physical and chemical characterization illustrate that these materials have different properties. MnO_x/GC formed a nanostructured morphology with α-$Mn_2^{III}O_3$ crystallinity.[13] MnO_x/Au-Si_3N_4, on the other hand, consists of densely packed needles, shown in Figure 2B, and has no long range atomic order as demonstrated by the absence of the x-ray diffraction peaks in Figure S7.

Ex-situ XPS

The observed differences in the morphology and crystallinity of MnO_x/GC and MnO_x/Au-Si_3N_4 suggest that MnO_x/Au-Si_3N_4 might assume a different surface oxidation state than MnO_x/GC despite identical preparation conditions. Previous 3C and 3D demonstrates that XPS can detect changes in the MnO_x/Au-Si_3N_4 surface after it is exposed to reaction conditions. Specifically, application of an ORR relevant potential of 0.7 V results in the elimination of $Mn^{II}O$ features and leads to $\Delta 2p_{1/2}$ and Δ3s values that are consistent with the formation of either Mn^{III} oxide or $Mn_3^{II,III,III}O_4$. Conclusive assignment to either phase is not possible using purely XPS because of the similarity between the $\Delta 2p_{1/2}$ and Δ3s of $Mn_2^{III}O_3$ and $Mn_3^{II,III,III}O_4$ shown in Figure S9. Application of an OER relevant potential of 1.8 V also results in the elimination of $Mn^{II}O$ features and leads to slight changes in $\Delta 2p_{1/2}$ and Δ3s values previously attributed to $Mn^{IV}O_2$ phase, indicating that the surface oxidation state under the OER conditions is likely a mixed valent $Mn^{III,IV}O_2$ oxide. These results provide further evidence that the MnO_x/Au-Si_3N_4 surface is unlike the surface of MnO_x/GC. While in both cases the oxidation state changes were expected upon exposure to the reaction conditions, these changes could not be detected with the MnO_x/GC catalyst using the same characterization procedure.[28] To monitor the oxidation state changes *in-situ* and gain structural information about the catalyst both before and after exposure to reaction conditions, we performed *in-situ* XAS experiments on a MnO_x/$AuSi_3N_4$ catalyst.

In-situ XAS under Electrochemical Reaction Conditions

XAS data were collected using a setup illustrated in Figure 1. Prior to collecting *in-situ* XAS measurements, cyclic voltammetry characterization of the catalyst was performed in air in ORR and OER potential windows of 0.05 V to 1.1 V and 0.05 V to 1.8 V. The resulting cyclic voltammetry behavior shown in Figure 4A is similar to the result obtained under standard laboratory conditions in oxygen saturated electrolyte (Figure 2A). The smaller magnitude of the ORR current obtained at beamline 10.3.2 can be explained by the smaller oxygen concentration in the air saturated electrolyte than the O_2 saturated electrolyte. The increase in the ORR current after exposure of the catalyst to OER potentials is attributed to the formation of oxygen bubbles on the surface of the catalyst and the resulting increase in local oxygen concentration. To acquire steady-state *in-situ* XAS data, the MnO_x/Au-Si_3N_4 catalyst was held at an ORR relevant potential of 0.7 ± 0.007 V or at an OER relevant potential of 1.8 ± 0.001 V in 0.1 M KOH. The resulting chronoamperometry curves are shown in Figures 4B and 4C. The smaller instability in the potential during the OER hold and the corresponding decreased level of noise in measured current density was due to a smaller ohmic resistance during the OER experiment. The occasional drops and recovery observed in the OER chronoamperometry data were likely due to formation and disappearance of oxygen bubbles from the surface. For comparison, XAS measurements were also performed on an as-prepared (dry) catalyst.

In-situ XANES

In-situ XANES measurements, shown in Figure 5A, follow the trend observed with *ex-situ* XPS characterization. When the dry electrode was set in the electrochemical cell and an ORR relevant potential of 0.7 V was applied, a negative shift was observed in the XANES spectrum (Figure 5A), showing a reduction in the Mn oxidation state. On the other hand, a subsequent change to OER conditions led to a shift in the edge position to a higher energy, indicating an increase in the Mn oxidation state. Figure 5B compares the XANES spectrum obtained under the ORR conditions to the spectra of $Mn^{II}O$, $Mn_3^{II,III,III}O_4$, $Mn^{III}OOH$, and alpha-$Mn_2^{III}O_3$ standards. The observed Mn valence in the catalyst during the ORR is less than 3, but greater than 2, closely matching the Mn valence of 2.7 observed in $Mn_3^{II,III,III}O_4$. Analysis of the MnO_x/Au-Si_3N_4 catalyst after exposure to an OER potential of 1.8 V, shown in Figure 5C, reveals that the MnO_x catalyst is more oxidized than the alpha-$Mn_2^{III}O_3$ phase, more reduced than beta-$Mn^{IV}O_2$, and exhibits strong similarity to the birnessite phase. Birnessite is a naturally occurring Mn mineral with a layered structure, which accommodates cations and water in the interlayer space. Its synthetic forms, such as triclinic Mg^{2+} birnessite whose spectrum is shown in Figure 5C, usually have 20-40% Mn^{III} in $Mn^{IV}O_2$,[29-32] with an average oxidation state of 3.6-3.8. In addition to birnessite, the XANES spectrum of the MnO_x/Au-Si_3N_4 catalyst poised at the OER potential also shows similarities to other $Mn^{III,IV}$ oxide phases that accommodate cations into the structure (Figure S10), such as todorokite and hollandite. We will consider the birnessite phase in our subsequent analysis of the OER catalyst, as several groups have shown that birnessite can be accessed electrochemically at room temperature,[33,34] while the formation of todorokite and hollandite requires additional thermal treatment or high pressure.[32,35]

Examination of the rising edge position of MnO_x/Au-Si_3N_4 catalyst under OER condition reveals that it is slightly lower than the rising edge position of the birnessite phase, indicating that the oxidation state of the OER catalyst is approximately 3.6. The lower oxidation state in the sample than in the birnessite standard can be attributed to the contribution of some electrochemically isolated domains of $Mn_3^{II,III,III}O_4$ that are not oxidized under OER conditions or to a higher percentage of Mn^{III} sites in the OER catalyst as compared to the standard. The XANES spectra of the OER catalyst was best fit with ~ 80% birnessite and ~ 20% $Mn_3^{II,III,III}O_4$ spectra, although it is difficult to specify the detailed composition of the minority species (Table S3 in SI). The presence of up to 20% $Mn_3^{II,III,III}O_4$ at potentials significantly beyond the thermodynamic potential at which Mn_3O_4 is expected to oxidize[36] can be explained either by $Mn_3^{II,III,III}O_4$ particles electronically isolated from the rest of the sample[37] or by $Mn_3^{II,III,III}O_4$ located in the interior of the film, away from solid-liquid interface.[22] More detailed discussion of these two possibilities is presented in the SI.

In-situ EXAFS

The EXAFS spectra of MnO_x/Au-Si_3N_4 shown in Figure 6A provide further information about the relevant phases. Accompanied by the oxidation state changes observed in the XANES spectra (Figure 5A), substantial changes were observed in the EXAFS spectra among as-prepared, 0.7 V, and 1.8 V MnO_x samples. The presence of significant peak intensity in the R' = 5Å region of the as-prepared MnO_x but not in the R' = 5Å region of 0.7 V and 1.8 V samples, likely originated from the Mn--Mn--Mn multiple scattering, suggesting that the as-prepared MnO_x has a more extended structure. The exact atomic arrangement in the as-prepared catalyst could not be identified because its EXAFS spectrum, which did not match any of the considered MnO_x standards, likely corresponded to a mixture of MnO_x phases. The presence of a mixture of phases is consistent with the results of the XPS analysis, which identified two different oxidation states on the surface of the as-prepared catalyst. EXAFS of MnO_x under ORR conditions was compared with reference

spectra of $Mn_3^{II,III,III}O_4$ and alpha-$Mn_2^{III}O_3$ in Figure 6B. The MnO_x/Au-Si_3N_4 shows much weaker EXAFS peak intensity than the $Mn_3^{II,III,III}O_4$ in the R' = 3Å region, despite the similarity in the XANES region. However, the EXAFS curve fitting results show that the ORR spectrum can be fit well with the $Mn_3^{II,III,III}O_4$ atomic distances with smaller N (coordination) numbers, when the Debye-Waller factors were fixed to those of $Mn_3^{II,III,III}O_4$ (Table S4 in SI). This can be explained by a smaller particle size as opposed to an extended crystalline material or by a distortion of the phase due to an increased amount of Mn^{II} as compared to a pure $Mn_3^{II,III,III}O_4$ phase. A change to the oxidative potential of 1.8 V leads to a structural rearrangement of the MnO_x catalyst and the emergence of similarities in the peak positions between the MnO_x OER catalyst and a birnessite phase as shown in Figure 6C. EXAFS curve fitting of the MnO_x OER catalyst was carried out using birnessite fit result as starting parameters (Table S4 in SI). This approach generated a good fit, but required smaller N values than those found for the reference birnessite compound. The smaller N values indicate the presence of non-diffracting, small particle domains as opposed to an extended crystalline material and suggest the presence of a minority phase, such as $Mn_3^{II,III,III}O_4$, in agreement with the XANES analysis. We note that based purely on EXAFS spectra, a todorokite tunnel structure, could have also generated a good fit.[7,38] As mentioned in the discussion of XANES, however, we considered the birnessite phase in our analysis because it can form electrochemically,[33,34] while the formation of todorokite requires an additional high temperature treatment.[32]

In-situ XANES to Assess Film Porosity

To understand if OER catalysis is limited to the top geometric layer of a dense film, or if it occurs throughout the catalyst layer of a porous film, we prepared a second MnO_x/Au-Si_3N_4 catalyst. The catalyst was synthesized by reducing the number of deposition cycles from nine to one, yielding a sample half as thick as measured using cross-sectional scanning electron microscopy (SEM), Figures 7A and 7B. Despite the factor of 2 difference in film thickness, the samples exhibit similar XANES spectra under both the ORR and the OER conditions (Figure 7C). As the spectra were collected by fluorescence, providing information on the entirety of these relatively thin films, the similarity in the spectra suggests that the catalytic film is porous enough for both samples to have the same fraction of the electrochemically accessible material, as illustrated in Figure 8. Comparison of the OER current at 1.8 V, presented in Figure 7D, reveals about a factor of two higher current for the thicker sample, indicating a direct relationship between the thickness of the catalytic film and the OER activity. This result provides further evidence that the catalyst film is highly porous, allowing the reaction to occur throughout the entire catalyst structure. In this structure, we expect the more oxidized $Mn^{III,IV}$ oxide to be in contact with electrolyte and participate in OER, and the more reduced $Mn_3^{II,III,III}O_4$ to be located in the interior of the catalyst, away from the solid-liquid interface, with no opportunity to participate in electrocatalysis. It is also possible, however, that $Mn_3^{II,III,III}O_4$ may remain un-oxidized at the surface of the catalyst, due to poor contact between $Mn_3^{II,III,III}O_4$ particles and the rest of the film, as discussed in the SI. Because the electronically isolated $Mn_3^{II,III,III}O_4$ would also be unable to participate in OER electrocatalysis, we can link the oxidized $Mn^{III,IV}$ oxide to the observed OER current.

Analysis of K^+ Intercalation

Because birnessite MnOx has layered structure that accommodates ions, it was important to consider potassium intercalation into the catalyst during the characterization in potassium hydroxide electrolyte. Previously, potassium intercalation into MnO_x has been reported both under ORR[39,40] and OER conditions.[41,42] A recent study has also demonstrated that potassium may have a favorable effect on OER by stabilizing the layered structure of MnO_x[43] To monitor possible intercalation we used ex-*situ* XPS measurements, which

provided the ratio of potassium to Mn on the surface of MnO_x/Au-Si_3N_4 catalyst after its exposure to 0.7 V and 1.8 V. Measurements were also performed on the as-prepared catalyst, in which no potassium cations could be present. Our results, shown in Figure S11, indicate that a small amount of -potassium, corresponding to one K^+ for every hundred Mn, intercalates into the catalyst after exposure to the OER conditions, while intercalation under ORR conditions is negligible. This amount is less than what is expected for the synthetic birnessites,[29,30,32] indicating that the MnO_x/Au-Si_3N_4 catalyst under the OER conditions is composed of Mn sites with and without intercalated K^+. Further investigation is necessary to determine the role of K^+ in OER catalysis.

Structural Transformations as a Function of Applied Potential

The *in-situ* XAS characterization of the MnO_x/Au-Si_3N_4 catalyst identified a structural transformation of the catalyst with changes in the applied potential. These results indicate that different phases form under the ORR and OER conditions. ORR potentials favor the formation of a disordered $Mn_3^{II,III,III}O_4$ phase with spinel-like structure shown in Figure 9A, while the OER potentials favor the formation of an oxidized MnO_x phase, bearing similarities to birnessite structure shown in Figure 9B, along with a less oxidized phase, likely corresponding to unchanged $Mn_3^{II,III,III}O_4$.

The presence of a highly disordered $Mn_3^{II,III,III}O_4$ phase at 0.7 V links $Mn_3^{II,III,III}O_4$ to the high activity for the ORR. Formation of the $Mn_3^{II,III,III}O_4$ phase at 0.7 V is expected based on thermodynamics,[36,44] but experiments show that this phase is not very kinetically accessible. Specifically, in base, the reduction of $Mn^{IV}O_2$ to $Mn_3^{II,III,III}O_4$ has been previously demonstrated only in highly concentrated KOH electrolytes[45,46] and has been characterized by poor electrochemical reversibility and conductivity.[45,47,48] Mechanistic studies in low concentration KOH electrolytes by Kozawa and Yeager, more applicable to the present investigation, have identified Mn(III) oxide as the final reduction product of $Mn^{IV}O_2$.[46] *In-situ* XAS characterization by Lima et al. of another ORR catalyst consisting of MnO_x dispersed in Vulcan carbon detected the presence of some $Mn_3^{II,III,III}O_4$ at a similar cathodic potential during the cathodic sweep, but in a mixture with a more oxidized Mn(III) phase, likely corresponding to $Mn^{III}OOH$.[4] The scarcity of reports of complete reduction of MnO_x to $Mn_3^{II,III,III}O_4$ under potentials relevant for ORR at pH 13 warrants further investigation of the reductive behavior of MnO_x/Au-Si_3N_4 and identification of the precise voltage at which the phase transition to $Mn_3^{II,III,III}O_4$ begins.

Electrochemical oxidation of the $Mn_3^{II,III,III}O_4$ phase to a phase similar to birnessite is not expected based on the early studies of MnO_x as battery electrodes, which have suggested that $Mn_3^{II,III,III}O_4$ is electrochemically inactive and cannot be oxidized.[4,45,47-49] Recent studies of MnO_x supercapacitors, however, have not only identified $Mn_3^{II,III,III}O_4$ as a phase with excellent electrochemical conductivity and redox properties,[50-53] but have also shown that it can transform into a layered structure of birnessite after 100-1000 of electrochemical cycles.[33,34,54] The ability of our catalyst to transform from $Mn_3^{II,III,III}O_4$ phase formed at 0.7 V to greater than 80% of birnessite-like phase after a single cycle to an OER relevant potential of 1.8 V, is likely explained by the small domain size of the crystallites in the catalyst and the disordered structure of the starting $Mn_3^{II,III,III}O_4$ phase. Our study provides the first evidence of the formation of MnO_x with a birnessite-like structure during the OER in alkaline environment. Considering that previous studies have also linked a mixed $Mn^{III,IV}$ oxide phase with similarities to birnessite to high OER activity in acidic nafion membrane[7] and neutral electrolytes,[16,55,56] our results suggest that the OER activity of the mixed $Mn^{III,IV}$ oxide may be independent of the pH environment. Further studies are necessary to determine the exact active site and the reaction mechanism.

CONCLUSIONS

Identifying the active sites in catalysis, one of the most challenging endeavors to undertake in the field, is critical to understanding and improving catalytic materials. *In-situ* X-ray absorption spectroscopy (XAS) studies were employed to investigate the active phases of a manganese oxide (MnO_x) catalyst supported onto Au-Si_3N_4 (MnO_x/Au-Si_3N_4) during electrochemical reaction conditions for the oxygen reduction reaction (ORR) and the oxygen evolution reaction (OER). The investigations identified a disordered $Mn_3^{II,III,III}O_4$ as a phase under ORR conditions, and a mixture of two MnO_x phases under OER conditions: an oxidized phase with a structure similar to that of birnessite and a more reduced phase, likely corresponding to unchanged $Mn_3^{II,III,III}O_4$. By studying catalyst films of different thicknesses, it was shown that OER catalysis must occur throughout the catalyst structure and not just at the top most geometric layer of the film, indicating excellent porosity of the films. Although we identify a mixture of a more oxidized phase and $Mn_3^{II,III,III}O_4$ under OER conditions, due to the oxidizing potentials necessary for the OER we expect the more reduced $Mn_3^{II,III,III}O_4$ to be located away from the solid-liquid interface with no opportunity to turn over the reaction and the more oxidized phase to be in contact with the electrolyte and be important to the observed OER catalysis. As the electrochemical properties of MnO_x are highly dependent on the starting MnO_x phase[45,57] and underlying support, it is important to continue *in-situ* investigations of different MnO_x materials under ORR and OER conditions to advance understanding of structural parameters and surface conditions that contribute to the high activity observed for the two reactions.

Supplementary Material

Refer to Web version on PubMed Central for supplementary material.

Acknowledgments

Catalyst development and electrochemical characterization were supported as part of the Center on Nanostructuring for Efficient Energy Conversion (CNEEC) at Stanford University, an Energy Frontier Research Center funded by the U.S. Department of Energy, Office of Science, Office of Basic Energy Sciences under Award Number DE SC0001060. SEM, XPS, and XRD were performed at the Stanford Nanocharacterization Laboratory (SNL) part of the Stanford Nano Shared Facilities. In situ XAS experiments were supported by the Joint Center for Artificial Photosynthesis, a DOE Energy Innovation Hub, supported through the Office of Science of the U.S. Department of Energy under Award Number DE-SC0004993, and performed at the Advanced Light Source (BL 10.3.2), Berkeley, under Contract DE-AC02-05CH11231. Portions of this research were carried out at the Stanford Synchrotron Radiation Lightsource, a Directorate of SLAC National Accelerator Laboratory and an Office of Science User Facility operated for the U.S. Department of Energy Office of Science by Stanford University. The SSRL Structural Molecular Biology Program is supported by the DOE Office of Biological and Environmental Research, and by the National Institutes of Health, National Institute of General Medical Sciences (including P41GM103393) and the National Center for Research Resources (P41RR001209). The authors thank Dr. Sung-Hyeon Baeck for providing beta-MnO_2 and alpha-Mn_2O_3 powders and Dr. Jakob Kibsgaard for assistance with Figure 9.

REFERENCES

(1). Peuckert M, Yoneda T, Betta RAD, Boudart M. J. Electrochem. Soc. 1986; 133:944.

(2). Mukerjee S, Srinivasan S, Soriaga MP, McBreen J. J. Electrochem. Soc. 1995; 142:1409.

(3). Lima FHB, Calegaro ML, Ticianelli EA. J. Electroanal. Chem. 2006; 590:152.

(4). Lima FHB, Calegaro ML, Ticianelli EA. Electrochim. Acta. 2007; 52:3732.

(5). Kanan MW, Yano J, Surendranath Y, Dinca M, Yachandra VK, Nocera DG. J. Am. Chem. Soc. 2010; 132:13692. [PubMed: 20839862]

(6). Bediako DK, Lassalle-Kaiser B, Surendranath Y, Yano J, Yachandra VK, Nocera DG. J. Am. Chem. Soc. 2012; 134:6801. [PubMed: 22417283]

(7). Hocking RK, Brimblecombe R, Chang LY, Singh A, Cheah MH, Glover C, Casey WH, Spiccia L. Nature Chem. 2011; 3:461. [PubMed: 21602861]

(8). Haas O, Holzer F, Müller S, McBreen JM, Yang XQ, Sun X, Balasubramanian M. Electrochim. Acta. 2002; 47:3211.

(9). Yeager E. J. Mol. Catal. 1986; 38:5.

(10). Mao LQ, Sotomura T, Nakatsu K, Koshiba N, Zhang D, Ohsaka T. J. Electrochem. Soc. 2002; 149:A504.

(11). Cao YL, Yang HX, Ai XP, Xiao LF. J. Electroanal. Chem. 2003; 557:127.

(12). Cheng FY, Su Y, Liang J, Tao ZL, Chen J. Chem. Mat. 2010; 22:898.

(13). Gorlin Y, Jaramillo TF. J. Am. Chem. Soc. 2010; 132:13612. [PubMed: 20839797]

(14). Morita M, Iwakura C, Tamura H. Electrochim. Acta. 1979; 24:357.

(15). El-Deab MS, Awad MI, Mohammad AM, Ohsaka T. Electrochem. Commun. 2007; 9:2082.

(16). Zaharieva I, Najafpour MM, Wiechen M, Haumann M, Kurz P, Dau H. Energy Environ. Sci. 2011; 4:2400.

(17). Tench D, Warren LF. J. Electrochem. Soc. 1983; 130:869.

(18). Gilbert B, Frazer BH, Belz A, Conrad PG, Nealson KH, Haskel D, Lang JC, Srajer G, De Stasio G. J. Phys. Chem. A. 2003; 107:2839.

(19). Barr TL, Seal S. J. Vac. Sci. Technol., A. 1995; 13:1239.

(20). Dicastro V, Polzonetti G. J. Electron. Spectrosc. Relat. Phenom. 1989; 48:117.

(21). Oku M, Hirokawa K, Ikeda S. J. Electron. Spectrosc. Relat. Phenom. 1975; 7:465.

(22). Djurfors B, Broughton JN, Brett MJ, Ivey DG. J. Electrochem. Soc. 2006; 153:A64.

(23). Marcus MA, MacDowell AA, Celestre R, Manceau A, Miller T, Padmore HA, Sublett RE. J. Synchrotron Radiat. 2004; 11:239. [PubMed: 15103110]

(24). Newville M. J. Synchrotron Radiat. 2001; 8:96. [PubMed: 11512993]

(25). Rehr JJ, Albers RC. Rev. Mod. Phys. 2000; 72:621.

(26). Webb SM, Tebo BM, Bargar JR. Am. Mineral. 90:1342.

(27). Burke LD, Osullivan JF. Electrochim. Acta. 1992; 37:585.

(28). Gorlin Y, Jaramillo TF. J. Electrochem. Soc. 2012; 159:H782.

(29). Post JE, Heaney PJ, Hanson J. Powder Diffr. 2002; 17:218.

(30). Post JE, Veblen DR. Am. Mineral. 1990; 75:477.

(31). Ching S, Petrovay DJ, Jorgensen ML, Suib SL. Inorg. Chem. 1997; 36:883.

(32). Golden DC, Chen CC, Dixon JB. Clays Clay Miner. 1987; 35:271.

(33). Dubal DP, Jagadale AD, Lokhande CD. Electrochim. Acta. 2012; 80:160.

(34). Dai Y, Wang K, Xie J. Appl. Phys. Lett. 2007; 90:104102.

(35). Shen YF, Zerger RP, DeGuzman RN, Suib SL, McCurdy L, Potter DI, O'Young CL. Science. 1993; 260:511. [PubMed: 17830429]

(36). Pourbaix, M. Atlas of Electrochemical Equilibria in Aqueous Solutions. Pergamon Press; 1966.

(37). Lowe MA, Gao J, Abruna HD. Journal of Materials Chemistry A. 2013; 1:2094.

(38). Manceau A, Gorshkov AI, Drits VA. Am. Mineral. 1992; 77:1144.

(39). Minakshi M. J. Electroanal. Chem. 2008; 616:99.

(40). Athouel L, Moser F, Dugas R, Crosnier O, Belanger D, Brousse T. J. Phys. Chem. C. 2008; 112:7270.

(41). Chigane M, Ishikawa M. J. Electrochem. Soc. 2000; 147:2246.

(42). Chigane M, Ishikawa M. J. Chem. Soc., Faraday Trans. 1998; 94:3665.

(43). Boppana VBR, Yusuf S, Hutchings GS, Jiao F. Adv. Funct. Mater. 2013; 23:878.

(44). Su H-Y, Gorlin Y, Man IC, Calle-Vallejo F, Norskov JK, Jaramillo TF, Rossmeisl J. Phys. Chem. Chem. Phys. 2012; 14:14010. [PubMed: 22990481]

(45). McBreen J. Electrochim. Acta. 1975; 20:221.

(46). Kozawa A, Yeager JF. J. Electrochem. Soc. 1965; 112:959.

(47). Boden D, Venuto CJ, Wisler D, Wylie RB. J. Electrochem. Soc. 1967; 114:415.

(48). Boden D, Venuto CJ, Wisler D, Wylie RB. J. Electrochem. Soc. 1968; 115:333.

(49). Nam KW, Kim MG, Kim KB. J. Phys. Chem. C. 2007; 111:749.

(50). Jiang J, Kucernak A. Electrochim. Acta. 2002; 47:2381.

(51). Djurfors B, Broughton JN, Brett MJ, Ivey DG. J. Mater. Sci. 2003; 38:4817.

(52). Zhang F, Zhang X-G, Hao L. Mater. Chem. Phys. 2011; 126:853.

(53). Lin Y-H, Wei T-Y, Chien H-C, Lu S-Y. Adv. Eng. Mater. 2011; 1:901.

(54). Dubal DP, Dhawale DS, Salunkhe RR, Lokhande CD. J. Electroanal. Chem. 2010; 647:60.

(55). Zaharieva I, Chernev P, Risch M, Klingan K, Kohlhoff M, Fischer A, Dau H. Energy Environ. Sci. 2012; 5:7081.

(56). Iyer A, Del-Pilar J, King'ondu CK, Kissel E, Garces HF, Huang H, El-Sawy AM, Dutta PK, Suib SL. J. Phys. Chem. C. 2012; 116:6474.

(57). Desai BD, Fernandes JB, Dalal VNK. J. Power Sources. 1985; 16:1.

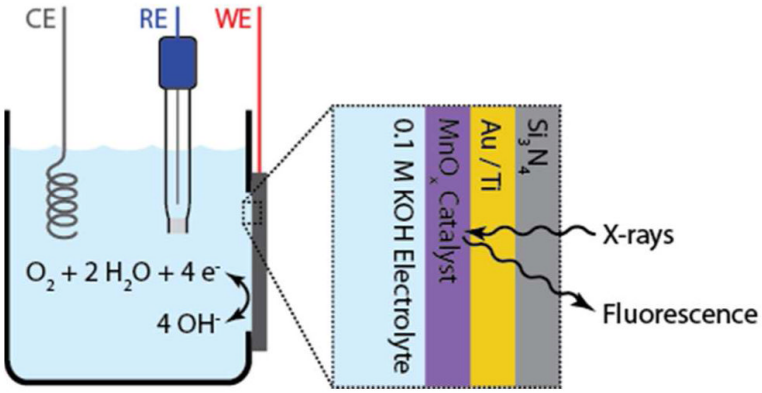

Figure 1.

In-situ XAS set-up, with the back-side of Si_3N_4 window facing the x-rays and the front side of the window, with electrodeposited MnO_x on a layer of Au/Ti facing the electrolyte. CE, RE and WE stand for counter, reference and working electrode, respectively.

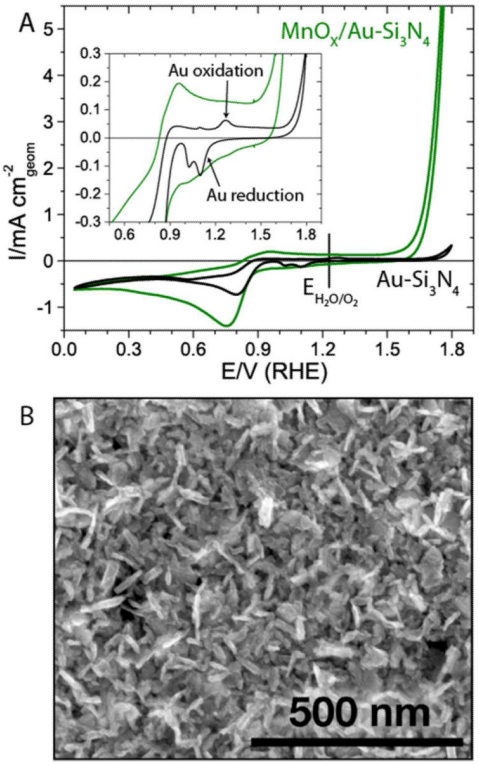

Figure 2.

A. Cyclic voltammetry of the MnO_x catalyst in O_2 showing bifunctional ORR/OER activity and the background activity of the Au-Si_3N_4 support. Inset shows the disappearance of Au redox features after addition of MnO_x; B. Scanning electron microscopy image illustrating needle-like morphology of MnO_x.

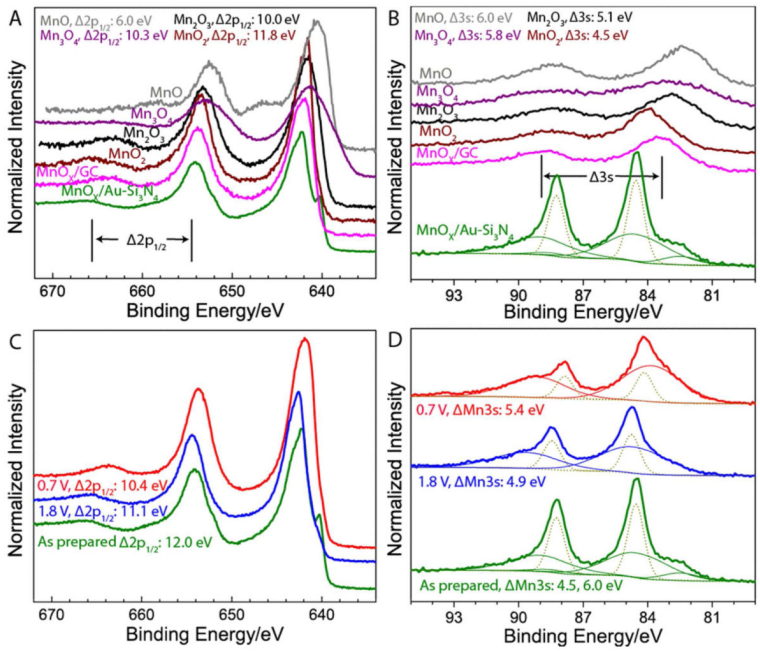

Figure 3.

A, B. Comparison of Mn 2p and Mn 3s spectra of MnO_x on Au-Si_3N_4 and glassy carbon supports to the spectra of MnO_2, Mn_2O_3, Mn_3O_4, and MnO powder standards. C, D. Comparison of Mn 2p and Mn 3s spectra of MnO_x on Au-Si_3N_4 support to the spectra of the same sample after exposure to ORR or OER relevant potentials.

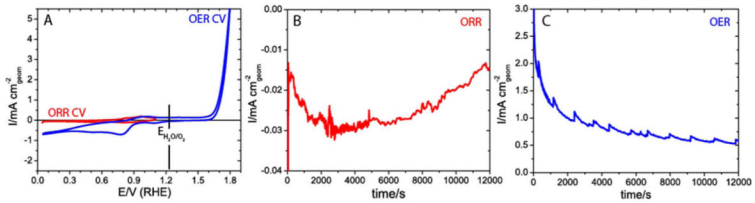

Figure 4.

A. Cyclic voltammetry of the catalyst performed prior to *in-situ* XAS measurements; B. Chronoamperometry at 0.7 V during *in-situ* XAS measurements at ORR relevant electrochemical conditions in air; C. Chronoamperometry at 1.8 V during *in-situ* XAS measurements at OER relevant electrochemical conditions in air.

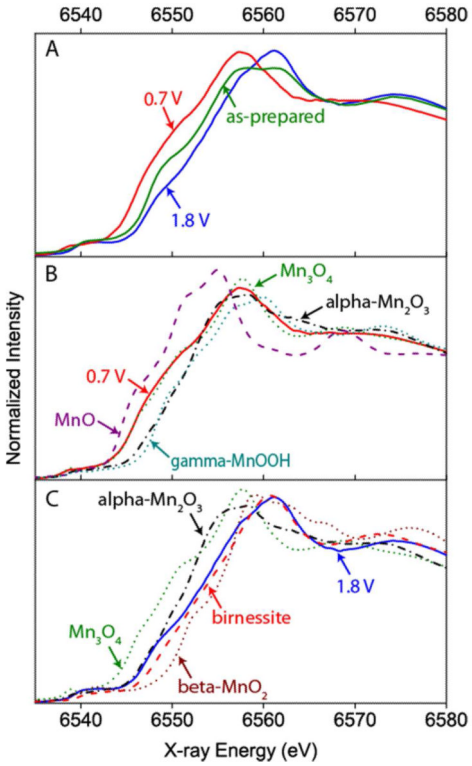

Figure 5.

A. Comparison of XANES data collected on as prepared MnO_x/Au-Si_3N_4 film and on MnO_x/Au-Si_3N_4 film after *in-situ* exposure to ORR and OER relevant conditions. B. MnO_x /Au-Si_3N_4 film poised at 0.7 V overlayed with MnO, Mn_3O_4, alpha-Mn_2O_3, and gamma-MnOOH. C. MnO_x /Au-Si_3N_4 film poised at 1.8 V overlayed with Mn_3O_4, alpha-Mn_2O_3, birnessite, and beta-MnO_2.

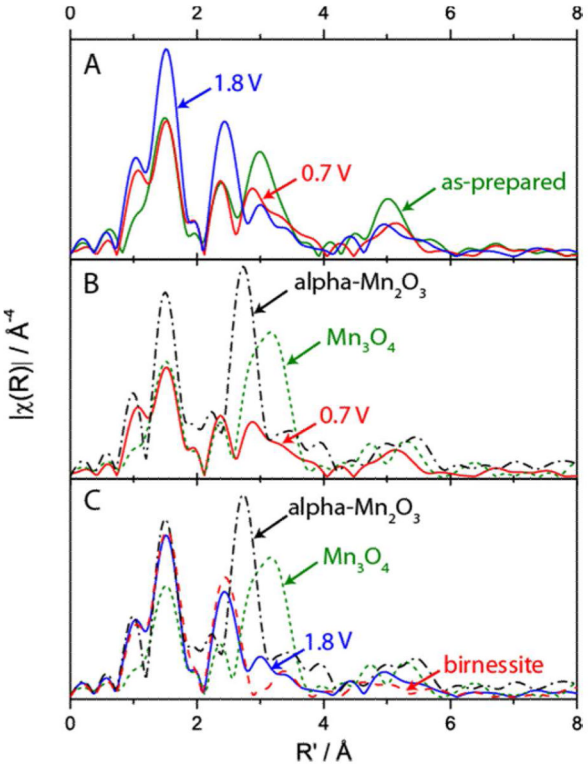

Figure 6.

A. Comparison of *in-situ* EXAFS collected on as-prepared MnO_x/Au-Si_3N_4 film and on MnO_x/Au-Si_3N_4 film after *in-situ* exposure to ORR andOER potentials. B MnO_x/Au-Si_3N_4 film poised at 0.7 V overlayed with Mn_3O_4 and alpha-Mn_2O_3. C. MnO_x/Au-Si_3N_4 film poised at 1.8 V overlayed with Mn_3O_4, alpha-Mn_2O_3, and birnessite.

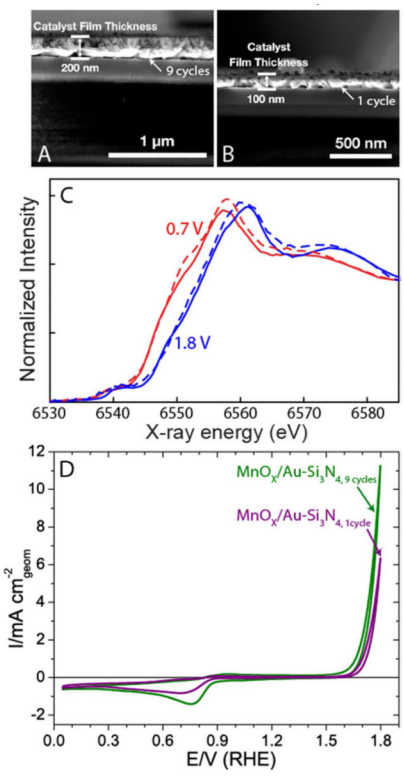

Figure 7.

A. Scanning electron microscopy (SEM) image of 200 nm MnO_x on Au-Si_3N_4 after 9 cyclic voltammetry (CV) cycles of deposition. B. SEM image of 100 nm MnO_x on AuSi_3N_4, demonstrating a 2 fold reduction in the thickness of MnO_x after the number of CV deposition cycles is lowered from 9 to 1. C. Comparison of XANES for 9 (solid lines) and 1 (dashed lines) cycle samples after exposure to ORR (red) and OER (blue) potentials. D. CV characterization of the ORR and the OER activities, illustrating that the OER activity scales with the thickness of MnO_x catalyst.

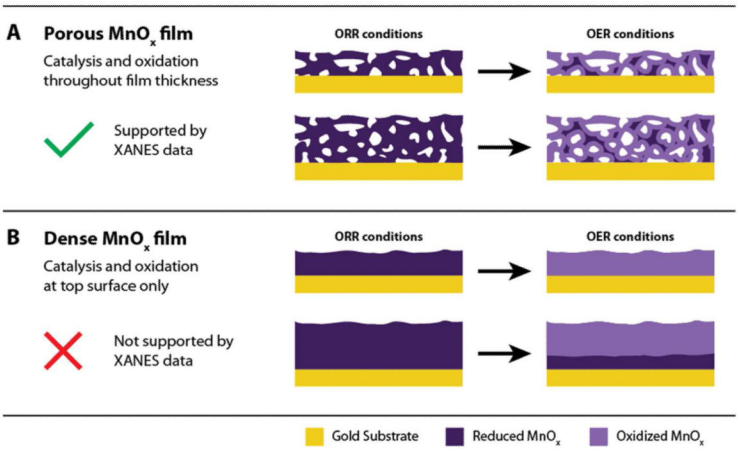

Figure 8.

A. Schematic of oxidation within a porous thin film, illustrating the same ratio of oxidized to reduced MnO_x for both thick and thin catalytic layers. B. Schematic of oxidation within a dense thin film, illustrating a higher ratio of oxidized to reduced MnO_x for a thinner film. The porous structure is consistent with XANES measurements presented in Figure 6C.

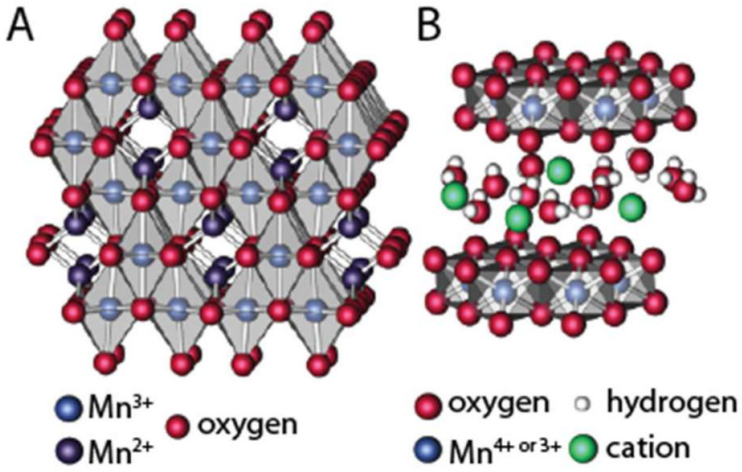

Figure 9.

Schematic showing the crystal structures of A. Mn_3O_4, which consists of octahedral (light blue) and tetragonal (dark blue) Mn sites, and B. M^{n+}-birnessite, which consists of sheets of edge-sharing MnO_6 octahedra with cations and water intercatalated into the interlayer space.